Rendiconti Lincei. Scienze Fisiche e Naturali
https://doi.org/10.1007/s12210-023-01165-1

Formation enthalpies of Al–Mn–Pd and the structure of the *i*-AlMnPd quasicrystal

Marek Mihalkovič[1] · Michael Widom[2]

Received: 27 February 2023 / Accepted: 17 May 2023

Abstract
This paper reports formation enthalpies of phases in the Al–Mn–Pd ternary alloy system as calculated from first principles using electronic density functional theory. We consider all crystal structures as reported in the assessed phase diagrams of the ternary and its binary alloy subsystems (Al–Mn, Al–Pd, and Mn–Pd), as well as additional reported or hypothetical structures. Icosahedral and decagonal quasicrystalline approximants are among the structures that we predict to be stable, or nearly so. Our results suggest the need for careful experimental reexamination of phase stability in each of the alloy systems, in tandem with further efforts to refine crystallographic and ab-initio structures.

Keywords Quasicrystal · Icosahedral Al–Mn–Pd · Structure · Enthalpy

1 Introduction

AlMnPd is one of the most studied quasicrystal forming systems. It has an icosahedral phase located around composition $Al_{70}Mn_{10}Pd_{20}$ and a decagonal phase close to $Al_{70}Mn_{20}Pd_{10}$ (Grushko et al. 1999). The icosahedral phase lies close in composition to the first-discovered quasicrystal (Shechtman et al. 1984), $Al_{86}Mn_{14}$, and it can be prepared by equilibrium methods (Boudard et al. 1995). Despite that, to-date no existing structure model passed the scrutiny of ab–initio evaluation of its stability against competing crystal phases, thus motivating the present study.

Specifically, we examine structures drawn from crystallographic experiment or based on theoretical models. In the event that these models do not uniquely specify the structure, we apply empirical interatomic interactions to refine chemical occupations through computer simulation. Then we employ accurate quantum mechanical total energy calculations to determine the relative stability of different structures at low temperature.

We match the assessed experimentally observed phases as reported by the American Society of Metals (ASM) with crystallographic structures as reported by the Inorganic Crystal Structure Database (ICSD). Our goal is to identify crystal structures for each reported phase, and to validate this identification through first-principles total energy calculations. Structures are identified through a combination of their Pearson names, space group and other identifiers. Phases are identified through their names, compositions, and other pertinent information. Icosahedral and decagonal quasicrystals are represented by "approximant" structures that spontaneously form during simulations.

Our calculated formation enthalpies reveal numerous conflicts with reports of structure and phase stability. The origins and potential resolutions of the conflicts are discussed. Remarkably, the only ternary structures predicted to be stable at low temperatures are large unit cell quasicrystalline approximants.

2 Methods

Our calculations follow methods outlined in a prior paper (Mihalkovič and Widom 2004). We utilize

This paper belongs to the topical collection "Quasicrystals: State of the art and outlooks" originated from an international conference organized by the Accademia dei Lincei, held in Rome on November 18, 2022 on the occasion of the 2022 International Year of Mineralogy.

✉ Michael Widom
widom@cmu.edu

[1] Institute of Physics, Slovak Academy of Sciences, 84511 Bratislava, Slovakia

[2] Department of Physics, Carnegie Mellon University, Pittsburgh, PA 15213, USA

Published online: 07 June 2023

VASP (Kresse and Furthmuller 1996) to carry out first principles density functional theory (DFT) total energy calculations in the PBE generalized gradient approximation (Perdew et al. 1996). We adopt projector augmented wave potentials (Blochl 1994; Kresse and Joubert 1999) and maintain a fixed energy cutoff of 270 eV (the default for Mn). All calculations involving Mn considered the possibility of spin polarization. As quasiperiodic structures do not obey the periodic boundary conditions required for DFT, quasicrystals will be modeled using large unit cell periodic approximants to minimize the boundary influence. We relax all atomic positions and lattice parameters using the Normal precision setting, and increase our k-point densities until energies have converged to within 1 meV/atom, then carry out a final static calculation using the tetrahedron integration method.

Given total energies for a variety of structures, we calculate the enthalpy of formation ΔH_{for} which is the enthalpy of the structure relative to a tie-line connecting the ground state configurations of the pure elements (Mihalkovič and Widom 2004). Formally, for a compound of stoichiometry $\text{Al}_x\text{Mn}_y\text{Pd}_z$ where $x + y + z = 1$, we define

$$\Delta H_{\text{for}} = H(\text{Al}_x\text{Mn}_y\text{Pd}_z) - (xH(\text{Al}) + yH(\text{Mn}) + zH(\text{Pd})) \tag{1}$$

where all enthalpies are per atom. Vertices of the convex hull of ΔH_{for} constitute the predicted low temperature stable structures. For structures that lie above the convex hull, we calculate the instability energy ΔE as the enthalpy relative to the convex hull.

Our structures are drawn from the ASM phase diagram database (ASM) and from the Inorganic Crystal Structure Database (ICSD), supplemented with original publications. When presented with multiple structure possibilities, or mixed site occupancy, we examine plausible structures and report the most energetically favorable. In cases where experiments or models do not fully specify the structure (e.g. in cases of partial or mixed chemical occupation) we refine structures using Monte Carlo annealing and relaxation subject to empirically oscillating pair potentials (Mihalkovič and Henley 2012). Our potentials are fitted to the form

$$V(r) = \frac{C_1}{r^{\eta_1}} + \frac{C_2}{r^{\eta_2}} \cos(k_* r + \phi_*) \tag{2}$$

with parameters as given in Table 1 and Fig. 1. We also perform Monte Carlo/molecular dynamics simulations supplemented with replica exchange (Mihalkovič and Widom 2020) to optimize quasicrystalline structures. All structures are then fully relaxed within DFT in order ot obtain accurate total energies.

One of our goals is to screen the experimentally assessed phase diagrams for conflicts with DFT evaluations of stability. We flag cases where the assessment claims low temperature (LT) or room temperature (RT) stability but DFT indicates an enthalpy lying above the convex hull. Since we neglect entropic effects, ΔE values of order $k_B T \approx 26$ meV/atom could conceivably be overcome, but more likely the reported crystallographic structure needs refinement, or more careful equilibration is required.

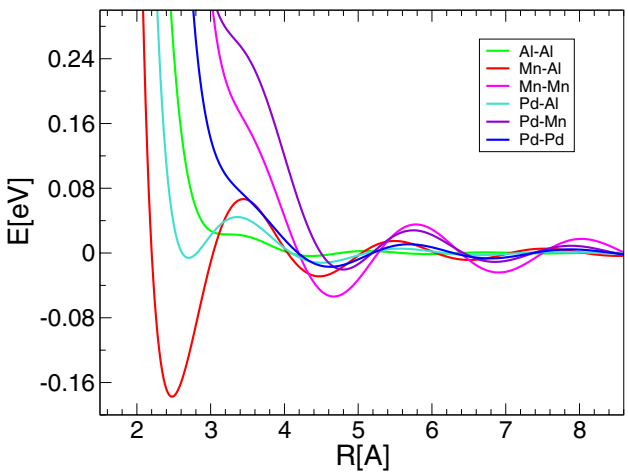

Fig. 1 Pair potentials as given by Eq. (2) with fitted parameters as in Table 1

Table 1 Fitted parameters for Al–Mn–Pd EOPP potentials

	C_1	η_1	C_2	η_2	k_*	ϕ_*
Al–Al	2497.0	9.9797	− 2.1972	4.1609	3.9470	1.5270
Al–Mn	35,935	15.683	3.9725	3.2700	3.1220	1.5137
Al–Pd	2052.7	10.211	5.9551	4.0744	3.0032	1.8990
Mn–Mn	1.3871×10^5	11.753	− 1.5400	2.1493	− 2.8182	0.7226
Mn–Pd	606.71	6.5741	− 6.2022	3.2063	− 3.0004	1.8224
Pd–Pd	16,446	10.572	− 1.0907	2.6558	− 2.9027	0.9748

3 Al–Mn–Pd ternary alloy system

To evaluate stability of a ternary alloy system we need to examine all three of its binary subsystems, as well as all three constituent elements.

3.1 Pure elements

Elemental Al and Pd each take the face centered cubic structure (FCC, Pearson type cF4, space group $Fm\bar{3}m$) at all temperatures up to their melting points. Mn, in contrast, takes one of the most complex elemental structures at low temperature, α-Mn (Pearson type cI58, space group $I\bar{4}3$ m), then passes through high temperature (HT) phases β-Mn (Pearson type cP20, space group $P4_132$) and γ-Mn (FCC) until reaching body centered cubic δ-Mn (BCC, Pearson type cI2, space group $Im\bar{3}m$). Our calculations find that α -Mn exhibits a type of antiferromagnetism, with moments of $2.6\mu_B$ on the 2a site and $-1.66\mu_B$ on the 8c sites. β- and γ-Mn prove at most weakly magnetic. δ-Mn favors ferromagnetism in its electronic ground state, although as a high temperature phase, it exists only above its hypothetical Curie point. In summary we find complete agreement between assessed and DFT-predicted stability of the three elements.

3.2 Binary subsystems

3.2.1 Al-Mn

The ASM assessed phase diagram of $Al_{1-x}Mn_x$ (ASM; Du et al. 2007) contains numerous line compounds (phases of precisely fixed composition) with complex structures in the range of $x_{Mn} = 0.08 - 0.28$. Our DFT-calculated enthalpies of formation (see Fig. 2, Table 2) validate the low temperature stable structures as $Al_{12}Mn$ as Pearson type cI26, Al_6Mn as Pearson type oC28, and $Al_{11}Mn_4$ as Pearson type aP15.

$Al_{57}Mn_{12}$.cP138 is a metastable icosahedral quasicrystal approximant that can be stabilized through the addition of Si (Cooper and Robinson 1966; Elser and Henley 1985). Its structure is a body-centered cubic packing of Mackay icosahedra with empty centers. The symmetry is reduced from BCC to primitive cubic by chemical ordering of the clusters' third shells.

The assessed diagram lists two phases (Kreiner and Franzen 1997; Shoemaker et al. 1989) λ-$Al_{230.8}Mn_{53.3}$.hP586 rt (space group $P6_3/m$) and μ-$Al_{226.6}Mn_{55}$.hP563 (space group $P6_3/mmc$). They lie close in composition and remain stable over an extended temperature range, which is thermodynamically improbable (Okamoto and Massalski 1991). Indeed, a more recent assessment (Grushko and Balanetskyy 2008) continues the debate over the precise details of the

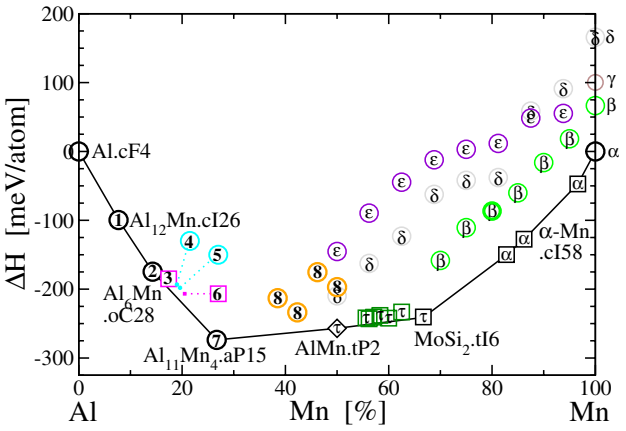

Fig. 2 Formation enthalpies of the Al-Mn alloy system. Plotting symbols are: heavy circle assessed RT/LT stable; light circle assessed HT stable; diamond assessed metastable; square hypothetical or unassessed structure. Stable structures on the convex hull are labeled. See Table 2 for details

phase diagram, with the main points of agreement that μ is more Mn-rich than λ and extends to higher temperature. The two phases are related by $a_\lambda = \sqrt{2}a_\mu$ and $c_\lambda = c_\mu/2$. All atoms in λ and μ belong to Mn-centered 13-atom icosahedral clusters, with the exception of two Al_9Mn clusters in which the Mn atoms are surrounded by tri-capped trigonal prisms. The icosahedra have various orientations, so we do not consider these phases as quasicrystal approximants. According to our calculations, neither is stable in the limit of low temperature. Both structures exhibit mixed or partial occupancy and hence should be regarded as high temperature phases. At slightly greater Mn concentration we have a decagonal quasicrystal approximant, Y-Al_3Mn.oP156 (Shi et al. 1994). Curiously, we find the energetically best structure of the Y-phase occurs at a composition close to Al_4Mn.

Several solid solutions with extended composition ranges exist beyond $x_{Mn} = 0.3$. The assessed Al15Mn11.hR26, also known as Al8Mn5.hR26 (Ellner 1990), is a high temperature phase up to ~50% Mn at which point it is assessed as stable down to low temperatures. DFT shows it could be HT stable but not LT, at least not with the site occupancy as indicated by experiment (Thimmaiah et al. 2017).

We find instead that a tP2 structure, assessed to be metastable, seems to be the true LT structure, with ferromagnetic order and $c/a > 1$. We also predict LT stability of an $AlMn_2$ .tI6 phase based on the prototype $MoSi_2$. This prototype is prevalent among Al-rich intermetallics (Mihalkovič et al. 2013) but has not been reported experimentally in Al-Mn, likely due to the metastability of the high temperature solid solution phases. The tP2 structure evolves continuously into tP6 through a sequence of layered structures alternating Al and Mn planes that we collectively label τ. Our DFT calculations show that the endpoints are LT stable, while

Table 2 Selected enthalpies of the Al–Mn binary system

Label	Phase name	Pearson symbol	Space group	ASM stability	DFT		
					x_{Mn}	ΔH	ΔE
1	$Al_{12}Mn$	cI26	$Im\bar{3}$	RT	7.7	− 98	− 6
2	Al_6Mn	oC28	Cmcm	RT	14.3	− 171	− 13
3	$Al_{57}Mn_{12}$	cP138	$Pm\bar{3}$	UN	17.4	− 182	14
4	λ-Al_4Mn	hP568	$P6_3/m$	**RT**	19.0	− 192	**17**
5	μ-Al_4Mn	hP563	$P6_3/mmc$	**RT**	19.6	− 198	**17**
6	Y-Al_3Mn	oP156	$Pna2_1$	UN	20.5	− 204	18
7	ν-$Al_{11}Mn_4$	aP15	$P\bar{1}$	RT	26.7	− 272	− 33
8	Al_8Mn_5	hR26	R3m	**RT**	50.0	− 194	**62**
τ	AlMn	tP2	P4/mmm	**MS**	50.0	− 256	**− 2**
τ	**$MoSi_2$**	tI6	I4/mmm	**UN**	66.7	− 240	**− 24**
25	ϵ-$Al_{55}Mn_{45}$	hP2	$P6_3/mmc$	HT	50.0	− 144	112
17	δ-$Al_{45}Mn_{55}$	cI2	$Im\bar{3}m$	HT	50.0	− 211	45
11	β-Mn	cP20	$P4_132$	**RT**	80.0	− 86	**79**
14	α-Mn	cI58	$I\bar{4}3$ m	**UN**	82.8	− 150	**− 2**

Labels specify plotting symbols on Fig. 2. Phase names are taken from ASM (ASM) or prototype. Space groups refer to observed symmetries and may differ from DFT realizations due to mixed or partial occupation. ASM stabilities are listed as RT if they extend to lowest reported ASM temperature, HT are high temperature only, and MS is assessed metastable. DFT energies (meV/atom) are formation enthalpy ΔH and stability relative to competing phases ΔE. Bolded stability and ΔE indicate conflicts between DFT and assessed stability. Bolded phase names indicate DFT predicted (UN indicates experimentally unknown) stable structures

the intermediate structures lie within 12 meV or less of the convex hull. AlMn.tP2 has magnetic moments of $2.3\mu_B$/Mn atom, while $AlMn_2$.tI6 is predicted to be nonmagnetic.

The highest temperature Mn phase, δ-Mn.cI2 extends in the assessed diagram from 40 to 100% Mn, but is interrupted by an hP2 structure in the range 55–75% Mn. Meanwhile, the HT β-Mn.cP20 phase extends at intermediate temperatures from 60 to 100% Mn, but becomes RT stable around 80% Mn. However, cP20 lies significantly above the convex hull over the entire composition range. Rather, the α -Mn.cI58 phase meets the convex hull if we substitute Al on the 2a site, the 8c site, or both. Presumably the β-Mn.cP20 variant is entropically stabilized at high temperatures and remains metastable down to low temperatures, preventing the observation of the more stable α variant.

We examined stability of the hP2 phase (not shown) and found that it lies strictly above cI2 for 50–85%Mn but falls below it in the limit of high Mn content. This behavior does not reproduce the experimental observation and likely shows the need for more rigorous approach to the *ab-initio* study of high temperature phases through inclusion of vibrational entropy, chemical substitution, or vacancies (Wolverton and Ozoliņš 2001; Mihalkovič and Widom 2020).

3.2.2 Al–Pd

The Al-rich region of the assessed diagram (ASM; Li et al. 2006) reports a hexagonal RT stable phase, Al_4Pd, of known lattice parameters but unknown structure. DFT finds the prototype Al_4Pt.hP102 is predicted nearly stable ($\Delta E = 9$ meV/atom) in a realization with 90 atoms, and it matches the experimental lattice parameters. The vacancies occur in mutually exclusive pairs of Al sites confined within channels, similar to those found in other transition metal aluminides (Mihalkovič and Widom 2012), and these can provide a source entropy that might stabilize the structure at elevated temperatures.

With increasing Pd concentration, the assessed diagram lists an orthorhombic HT stable Al_3Pd phase with known lattice constants but unknown structure. We checked a reported 16 Å periodic decagonal structure (Hiraga et al. 1994), ξ', with similar lattice constants and found it to be unstable by just $\Delta E = 23$ meV/atom. That is sufficiently close to the convex hull that it could be stabilized by the entropy of mixed and partial occupation.

We also tested the stability of the reported metastable crystal structure Al_2Pd.cF12 and find it to be unstable by $\Delta E = 39$ meV/atom. δ-Al_3Pd_2.hP5 is LT according to both the assessed diagram and DFT. The assessed diagram lists two $Al_{21}Pd_8$ phases, one is orthorhombic and is HT stable but no structure is given; the other is LT stable with structure tI116. DFT confirms LT stability of tI116.

One phase diagram (Li et al. 2006) lists a single HT phase from 45 to 55% Pd, while another (Okamoto 2003) lists the same HT phase, plus two RT phases that are listed without offering structures. Other

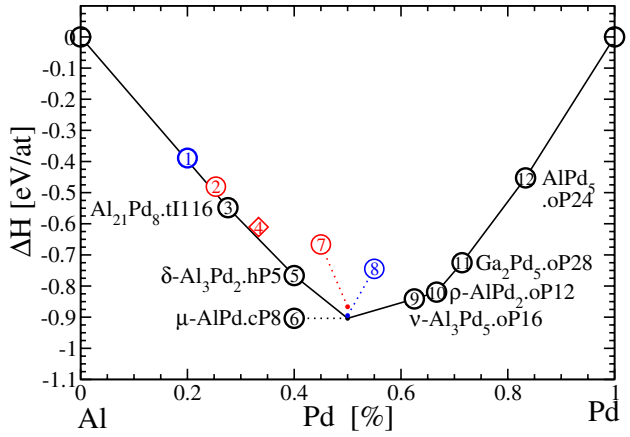

Fig. 3 Formation enthalpies of the Al–Pd alloy system. Plotting symbols as in Fig. 2. See Table 3 for details

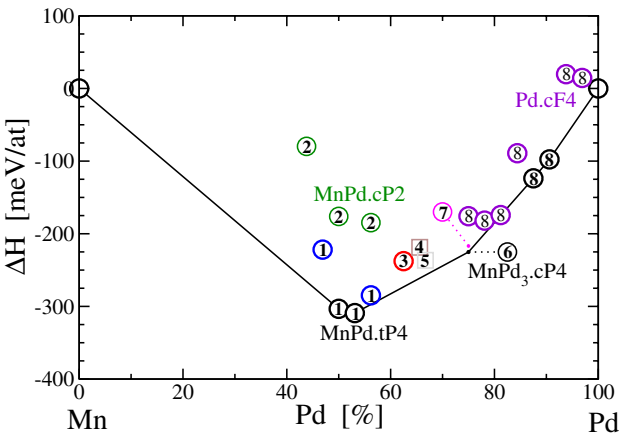

Fig. 4 Formation enthalpies of the Mn–Pd alloy system. Plotting symbols as in Fig. 2. See Table 4 for details

references (Matkovic and Schubert 1977; Ferro et al. 1964) list AlPd.cP8 (Al-rich) and AlPd.hR26. DFT finds stoichiometric AlPd.cP8 to be stable and AlPd.cP2 and β-AlPd.hR26 to be potentially HT. Curiously, all three AlPd phases are canonical cell tilings (CCT (Henley 1991)) in which Al atoms occupy even nodes, and Mn occupy odd nodes. β- and μ- are ABC tilings, while the cP2 structure is a pure A tiling.

At 62–72% Mn, the assessed diagram claims ν-Al_3Pd_5 .oP16 is HT but DFT predicts it to be LT stable. DFT confirms stability of ρ-$AlPd_2$.oP12. The RT Al_2Pd_5 phase has no assessed structure, but DFT predicts prototype Ga_2Pd_5.oP28 to be stable. Finally, Pd.cF4 exists as a solid solution from 80–100% Pd.

3.2.3 Mn–Pd

The Mn–Pd phase diagram (ASM; Okamoto 1993) is dominated by four phases with broad composition ranges. Generically, such phases should either exist only at high temperatures, or else they should narrow to a single specific composition at low temperature. This is because either chemical substitution or vacancies are required to create a composition range, and these would create entropy in the limit $T \rightarrow 0$K, violating the third law of thermodynamics (Abriata and Laughlin 2004; Okamoto and Massalski 1991).

Around 50% Pd the assessed diagram shows a low temperature phase MnPd.tP2. DFT verifies this structure to be stable but with antiferromagnetic order creating a $\sqrt{2} \times \sqrt{2}$ cell, hence the Pearson type tP4. There is also a HT phase MnPd.cP2; DFT finds this phase to be unstable by $\Delta E = 145$

Table 3 Selected enthalpies of the Al–Pd binary system

Label	Phase name	Pearson symbol	Space group	ASM stability	DFT		
					x_{Pd}	ΔH	ΔE
1	λ-Al_4Pd	hP102	P3c1	**RT**	25.0	− 389	**9**
2	ξ'-Al_3Pd	oP300	$Pna2_1$	HT	25.3	− 481	23
3	$Al_{21}Pd_8$	tI116	$I4_1/a$	RT	27.6	− 549	− 16
4	Al_2Pd	cF12	$Fm\bar{3}m$	MS	33.3	− 611	39
5	δ-Al_3Pd_2	hP5	$P\bar{3}m1$	RT	40.0	− 766	− 21
6	μ-AlPd	cP8	$P2_13$	RT	50.0	− 904	− 9
7	AlPd	cP2	$Pm\bar{3}m$	HT	50.0	− 867	37
8	β-AlPd	hR26	$R\bar{3}$	**RT**	50.0	− 895	**9**
9	ν-Al_3Pd_5	oP16	Pbam	HT	62.5	− 841	− 1
10	ρ-$AlPd_2$	oP12	Pnma	RT	66.7	− 820	− 32
11	**Ga_2Pd_5**	oP28	Pnma	RT	71.4	− 725	− 10
10	$AlPd_5$	oP24	Pnma	RT	83.3	− 453	− 30

Labels specify plotting symbols on Fig. 3. Other details as in Table 2

Table 4 Selected enthalpies of the Mn–Pd binary system

Label	Phase name	Pearson symbol	Space group	ASM stability	DFT		
					x_{Pd}	ΔH	ΔE
1	MnPd	**tP4**	P4/mmm	RT	50.0	− 303	− 12
2	MnPd	cP2	$Pm\bar{3}m$	HT	50.0	− 176	127
3	Mn_3Pd_5	oC16	Cmmm	**RT**	62.5	− 238	**35**
4	$Mn_{11}Pd_{21}$	tP32	P4/mmm	??	65.6	− 219	42
5	$MnPd_2$	oP12	Pnma	??	66.7	− 237	21
6	$MnPd_3$	cP4	$Pm\bar{3}m$	HT	75.0	− 225	− 8
7	Al_3Zr	tI16	I4/mmm	**RT**	75.0	− 217	**8**
8	Pd	cF4	$Fm\bar{3}m$	**RT**	75.0	− 176	**49**

Labels specify plotting symbols on Fig. 4. Other details as in Table 2

meV/atom suggesting possible metastability. The assessed diagram lists Mn_3Pd_5.oC16 as RT, but DFT predicts it to be unstable by $\Delta E = 27$ meV/atom suggesting possible entropic stabilization at HT. ASM also lists a stable Mn-rich variant of Mn_3Pd_5 with unknown structure.

At 75% Pd, ASM lists two different $MnPd_3$ phases as stable: one at the low Pd limit of an FCC solid solution, and also one with prototype Al_3Zr.tI16 (Rodic et al. 1991). We predict both to be unstable or HT. Finally, the assessed diagram shows the FCC solid solution as RT over the range 75–100% Pd. DFT instead predicts a sequence of optimized tetragonal structures at greater Pd % that lie on or near the convex hull. At the low Pd limit, $MnPd_3$, ASM lists cP4 at HT, but DFT predicts it to be stable.

3.3 Ternary Al–Mn–Pd

In contrast to the complexity of the binaries, the reported ternary phase diagram is relatively simple. Its dominant feature is a broad composition range of cubic Al_2(Mn,Pd) extending from AlMn up to AlPd. According to our DFT calculations, this phase does not remain stable at low temperatures. Instead, the AlMn.cI2 binary is a disordered high temperature BCC solid solution, and AlPd.cP2 is also a high temperature phase. We also confirm the HT solubility of Mn replacing Pd in the $Al_{21}Pd_8$ structure. The convex hull of our calculated enthalpies is shown in Fig. 5, along with a close-up of the Al-rich quasicrystal-forming region (Table 5).

We find that T-Al_3(MnPd).oP156, a 12 Å periodic decagonal approximant, is stable in the vicinity of the observed Al-Mn-rich decagonal quasicrystal phase. Indeed, its structure can be recognized as a decagonal quasicrystal approximant. As in the case of its binary counterpart, we find the optimal composition is close to Al_4(Mn,Pd). A closely related R-phase (not shown) is energetically nearly degenerate. Electron microscopy images of the decagonal phase reveal ~20 Å decagonal clusters (Hiraga and Sun 1993) that are too large to be observed in our T- and R-phases, which consist of alternative arrangements of hexagon-shaped tiles.

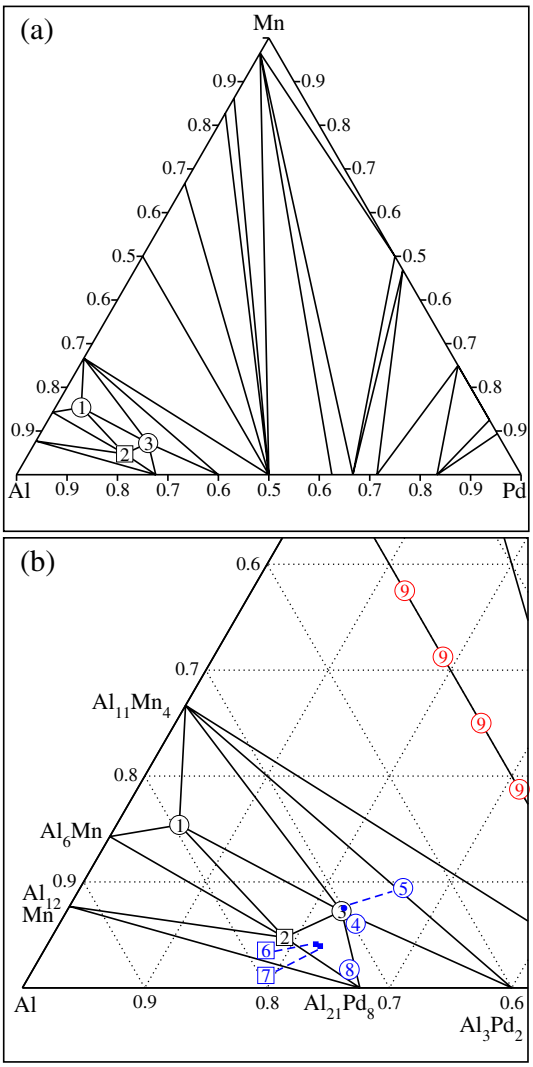

Fig. 5 Convex hull (**a**) and Al-rich phases (**b**) of the Al–Mn–Pd alloy system. Plotting symbols as in Fig. 2

Table 5 Selected enthalpies of the Al–Mn–Pd ternary system

Label	Phase name	Pearson symbol	Space group	ASM stability	DFT			
					x_{Mn}	x_{Pd}	ΔH	ΔE
1	T-Al_3(MnPd)	oP156	Pnma	ST	15.4	5.1	− 285	− 11.5
2	Al–Mn–Pd–Si	oP168	Pnma	UN	4.8	19.0	− 438	− 2.5
4	*i*-1/1 2 × 2 × 2	oP240	Pbcm	UN	6.7	20.0	− 463	10.5
4	*i*-2/1	aP128	F$\bar{5}$32	UN	7.0	21.1	− 493	3.3
3	*i*-3/2	aP552	F$\bar{5}$32	ST	7.2	22.5	− 523	− 2.7
5	*i*-5/3	aP2338	F$\bar{5}$32	UN	7.5	22.5	− 521	3.9
6	ϵ_{16}	aP399	P10_5/mmc	UN	4.0	22.1	− 483	2.4
7	ξ'	oP308	Pnma	UN	3.9	22.4	− 489	1.8
8	$Al_{21}Pd_8$	tI116	$I4_1$/a	ST	1.7	25.9	− 531	1.9
9	Al_2MnPd	cP2	Pm$\bar{3}$m	ST	25.0	25.0	− 539	41

Labels specify plotting symbols on Fig. 5. ST indicates stable at 840C. Other details as in Table 2

On the Al-Pd-rich side, we find a stable oP168 structure, and coexistence of the icosahedral and 16 Å-periodic decagonal quasicrystals and their approximants. The stable *oP*168 structure is derived from Sugiyama's quaternary AlMnPdSi. oP168 phase (Simura et al. 2011) by Si→Al substitution. At the first glance, this structure looks like a peculiar decagonal relative of the 16 Å decagonal quasicrystal family: viewed down the 24 Å-periodic *b* axis, it reveals pentagonal motifs. The ∼24 Å period is a sixfold multiple of the 4 Å periodicity characteristic of decagonal Al–TM quasicrystals, and its other lattice parameters relate to the 16 Å–decagonal approximant ξ' as c=7.6 Å∼ $c_{\xi'}/\tau$ and a=14.4∼ $\tau c_{\xi'}$. Here, τ denotes golden mean $(1+\sqrt{5})/2$. Closer inspection reveals that the structure contains no icosahedra, but rather Al_9 Pd, Al_{10}Pd and Al_{10}Mn clusters, of which none possesses a second shell with a clear pentagonal or icosahedral signature. Thus the most natural relatives of this structure are the binary Al_4Pd or $Al_{21}Pd_8$ structures.

"Pseudo-Mackay" (*pMI*) clusters are a fundamental motif of the 16 Å-decagonal and icosahedral families. They are composed of inner-shell Al_9Mn or Al_{10}Mn clusters, and an outer shell containing a large (Mn,Pd) icosahedron with an a_5 ∼4.56 Å fivefold radius, and 30 Al atoms about halfway between pairs of nearby transition-metal atoms, as in Fig. 6a, b. The decagonal family is represented by two nearly stable approximants: ξ' sometimes also denoted ϵ_6, and a larger, 400 atom/cell approximant denoted ϵ_{16}. The ξ' phase can be grown as a single crystal (Boudard et al. 1996). Its diffraction-refined structure contains unresolved fractional occupancy related to the secondary *pMI* structure of the *pMI* inner-core shells. The secondary structure was established by ab-initio methods (Frigan et al. 2011), and the whole 16 Å-decagonal family was described as a decorated Hexagon-Boat-Star tiling (Mihalkovič et al. 2017). The ϵ_{16} approximant is the lowest energy large approximant that fairly represents the metastable decagonal quasicrystal phase.

We model icosahedral phase structures in two ways. First, as a decoration of the canonical-cell tiling with twofold linkage length $b = 2\tau a_5/\sqrt{\tau+2}$ ∼7.76 Å, placing Mn-centered *pMI* clusters at even tiling vertices and Al_{12}Pd icosahedra (*I*-clusters) at odd vertices. Second, as structures that form

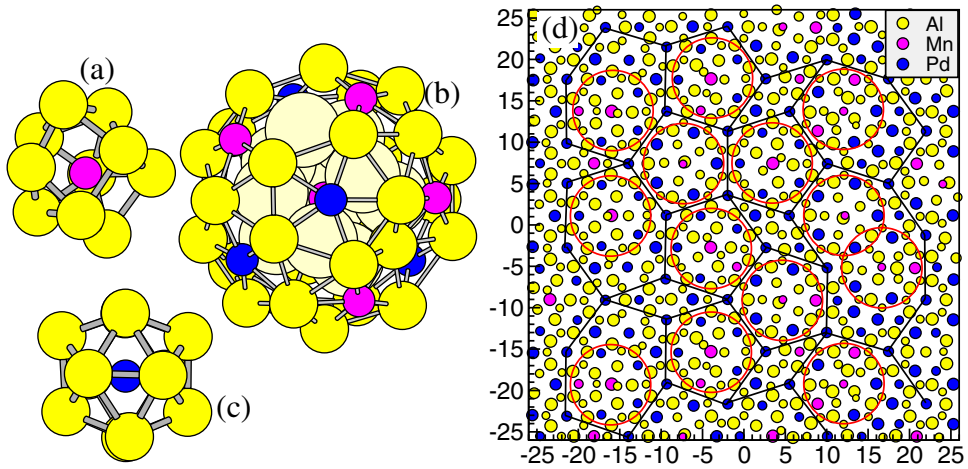

Fig. 6 Mn-centered clusters: **a** inner $Al_{9/10}$Mn and **b** outer Mackay shell; **c** Al_{12}Pd cluster; **d** 4A thick slice normal to (pseudo) fivefold axis through 2338-atom "5/3" approximant with pseudo-Mackay clusters outlined in red circles. A 7.8 Å tiling is shown connecting Al_{12}Pd clusters along twofold linkages

spontaneously in our atomistic simulations. We label the approximants with a ratio of successive Fibonacci numbers F_{n+1}/F_n, with 128 atoms for "2/1" up to 552 for "3/2", and 2338 for "5/3". Our naming convention is drawn from the definition of Henley's canonical cells designed for packing icosahedral clusters (Henley 1991). The $2 \times 2 \times 2$ supercell of the *i*-1/1 approximant is a decoration of the pure A-cell tiling, inspired by $Al_{11}Ir_4$ phase modeling (Mihalkovič and Henley 2013), and it is the only deterministic, regular structure among our icosahedral approximants. The 2/1 approximant is a decoration of the cubic ABC tiling with four *pMI* and four *I*-clusters per unit cell, with its secondary structure—correlations in orientation and variations of the inner-core $Al_{10}Mn$ or Al_9Mn clusters inside the *pMI* — optimized through simulation at $T = 500$ K. The two large approximants 3/2 and 5/3 are chemically disordered structures that spontaneously form at high temperatures in the simulations.

The resulting 3/2 and 5/3 approximant structures prove that the Mn-centered *pMI* and *I* clusters (Fig. 6a–c) are the two fundamental building blocks. In the figure, panel (d) shows a spontaneously formed tiling with icosahedra connected along twofold linkages; *pMI* clusters with Al_9Mn or $Al_{10}Mn$ inner cores are outlined as red circles. Note that, occasionally, four *I* clusters form skinny rhombus tile, with short body diagonal distance $b/\tau \sim 4.80$ Å: such cluster–cluster distance is forbidden in CCT. Also, analysis of the 3/2 and 5/3 approximants reveals that *I*-clusters are more prevalent than *pMI* . While the total number of clusters nearly matches the expected number of CCT nodes, the frequency ratio of the two clusters is about τ:1 in favor of $Al_{12}Pd$ *I*-clusters, instead of 1:1 as in a CCT-based model. The $2 \times 2 \times 2$–3/2 approximant crystal in the quaternary AlPd(CrFe), with around 4400 atoms in cubic cell (Fujita et al. 2013)—is entirely tiled by all four kinds of canonical cells, providing a strong argument in favor of the CCT geometry. Thus, while our simulations produce structures with favorable DFT enthalpies, they might not capture more regular (lower entropy, but also lower energy) realizations of the quasicrystal structure.

For comparison, we re-computed total energies of other icosahedral phase models. The Elser's (Quandt and Elser 2000) model and Zijlstra's (Zijlstra et al. 2005) revision of it (both in 65-atom primitive cells at the same composition) are at +45 and +18 meV/atom respectively. Elser's model shares the same building blocks and twofold linkages as CCT, but arranges them on alternating Penrose tiling nodes—hence *pMI* and *I*-clusters are linked by fivefold τa_{qc} ~7.38 Å long *pMI -I* linkages. The studied approximant is not sufficiently representative, and there remain unprobed aspects of the model that would only appear in larger approximants.

Krajčí et al. (1995) applied chemical ordering, inspired by Boudard et al. Boudard et al. (1992), to the 6D Katz-Gratias (KG) atomic structure (Gratias et al. 2000). The 544-atom "3/2 approximant" implementation of the model structure lies at +30 meV/atom after relaxation (not shown). The CCT and 6D model share an underlying cluster network: *pMI –pMI* and *I–I* connect along twofold *b*-linkages, and *pMI –I* connect along threefold $b\sqrt{3}/2$ linkages. Larger approximants possess short fivefold *pMI -I* linkages with length a_q. The KG model contains low-coordination Al_7Mn local environments instead of Al_8Mn or Al_9Mn mini-clusters, half of which are inner-cores of the *pMI* . Molecular dynamics annealing at moderate temperatures lowers the energy by up to 10 meV/atom, while introducing displacements up to 1.6 Å. Finally, we note that the *I* clusters of the KG model form inner shells of the so called "Bergman" or "mini-Bergman" clusters. The outer dodecahedral shell of this cluster displays chemical symmetry breaking dictated by sharing atoms with nearby *pMI* clusters.

Our stable icosahedral 3/2 approximant has composition $Al_{388}Mn_{40}Pd_{124}$, for a total of 552 atoms, making it the largest known quasicrystal approximant that is predicted to be LT stable according to DFT. As is frequently observed in Al-rich quasicrystals, the Fermi energy lies within a pseudogap region of the electronic density of states. However, in contrast to the case of i-AlCuFe (Mihalkovič and Widom 2020), where E_F lies very close to the pseudogap minimum, in i-AlMnPd E_F lies slightly below minimum in the energetically optimal structure (see Fig. 7). In the 5/3 approximant, with slightly higher energy, the pseudogap is less deep and further above E_F, suggesting that it might be possible to further reduce the energy through chemical substitution.

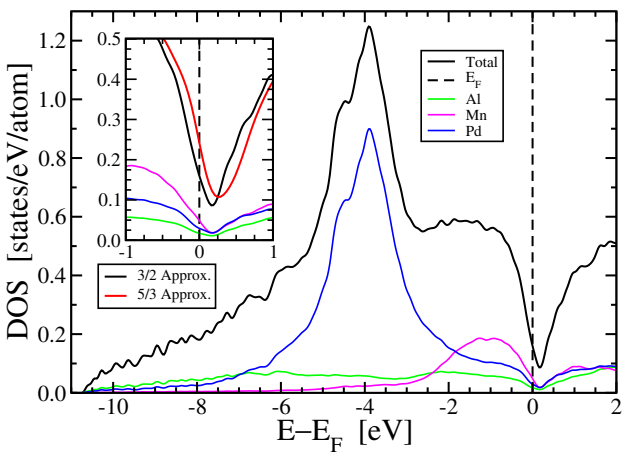

Fig. 7 Electronic density of states for $Al_{388}Mn_{40}Pd_{124}$ (black) and $Al_{390}Mn_{40}Pd_{122}$ (inset, red). Partial densities of states show the projected contributions of Al (green), Mn (magenta), and Pd (blue) to the total density of states/atom

4 Conclusion

We have surveyed the stability of most reported structures in the Al–Mn–Pd alloy system and its three binary subsystems. Although we find agreement between calculated formation enthalpies and experimentally assessed phase diagrams in the majority of cases, we find conflicts in roughly 1/3 of binary phases. In the case of the ternary, no reported crystal structure is predicted to be stable, while large quasicrystalline approximants appear to constitute the ternary ground states. Conflicts between experiment and calculation can indicate a failure of the experiments to distinguish low- and high-temperature stability (see, e.g. Ref. Wolverton and Ozoliņš (2001)), and metastability.

Alternatively, the conflicts could indicate that the calculated structure incorrect, possibly as the result of incomplete optimization of mixed or partial site occupation or lack of a suitable crystallographic refinement. Some conflicts may be due to the lack of quantum zero-point and finite temperature (entropic) corrections such as thermal vibrations or chemical substitution. Most of the discrepancies lie beyond the likely calculational errors due to the density functional and pseudopotential approximations.

This work highlights numerous areas requiring further experimental and theoretical investigation. Matching the ASM-assessed phase diagrams with ICSD-reported crystal structures is itself a challenge, but it allows the claims of phase stability to be tested through first principles calculation. This process provides a rich source of important experimental and theoretical research opportunities. Such an approach could be beneficially applied broadly across all alloy systems.

Icosahedral approximant structures may be found online at Ref. Mihalkovic and Widom (2023).

Acknowledgements MM is thankful for the support from the Slovak Grant Agency VEGA (No. 2/0144/21) and APVV (No. 20-0124, No. 19-0369). MW was supported by the Department of Energy under Grant No. DE-SC0014506. This research also used the resources of the National Energy Research Scientific Computing Center (NERSC), a US Department of Energy Office of Science User Facility operated under contract number DE-AC02-05CH11231 using NERSC award BES-ERCAP24744.

Funding Open Access funding provided by Carnegie Mellon University.

References

Abriata JP, Laughlin DE (2004) The third law of thermodynamics and low temperature phase stability. Prog Mater Sci 49:367

Blochl PE (1994) Projector augmented-wave method. Phys Rev B 50:17953

Boudard M, de Boissieu M, Janot C, Heger G, Beeli C, Nissen HU, Vincent H, Ibberson R, Audier M, Dubois JM (1992) Neutron and x-ray single-crystal study of the alpdmn icosahedral phase. J Phys Condens Matter 4:10149

Boudard M, Bourgeat-lami E, de Boissieu M, Janot C, Durand-charre M, Klein H, Audier M, Hennion B (1995) Production and characterization of single quasicrystals of the Al–Pd–Mn icosahedral phase. Philos Mag Lett 71:11

Boudard M, Klein H, Boissieu MD, Audier M, Vincent H (1996) Structure of quasicrystalline approximant phase in the al[sbnd]pd[sbnd]mn system. Philos Mag A 74:939

Cooper M, Robinson K (1966) The crystal structure of the ternary alloy alpha-(Al Mn Si). Acta Cryst 20:614

Du Y, Wang J, Zhao J, Schuster J, Weitzer F, Schmid Fetzer R, Ohno M, Xu H, Liu Z, Shang S, Zhang W (2007) Reassessment of the Al–Mn system and a thermodynamic description of the Al–Mg–Mn system. Int J Mater Res 98:855

Ellner M (1990) The structure of the high-temperature phase MnAl(h) and the displacive transformation from MnAl(h) into Mn5Al8. Metall Trans A 21:1669

Elser V, Henley CL (1985) Crystal and quasicrystal structures in Al–Mn–Si alloys. Phys Rev Lett 55:2883

Ferro R, Mattace Raso M, Rambaldi G, Bonino GB (1964) Ricerche sulle leghe dei metalli nobili con gli elementi piu elettropositivi. ix. la fase tipo B20 nel sistema di leghe alluminio-palladio. Atti Accad Naz Lincei 36:498

Frigan B, Santana A, Engel M, Schopf D, Trebin H-R, Mihalkovič M (2011) Low-temperature structure of ′-Al–Pd–Mn optimized by ab initio methods. Phys Rev B 84:184203

Fujita N, Takano H, Yamamoto A, Tsai A-P (2013) Cluster-packing geometry for Al-based F-type icosahedral alloys. Acta Crystallogr Sect A 69:322

Gratias D, Puyraimond F, Quiquandon M, Katz A (2000) Atomic clusters in icosahedral F-type quasicrystals. Phys Rev B 63:024202

Grushko B, Balanetskyy S (2008) A study of phase equilibria in the Al-rich part of the Al–Mn alloy system. Int J Mater Res 99:1319

Grushko B, Yurechko M, Tamura N (1999) A contribution to the Al–Pd–Mn phase diagram. J Alloys Compd 290:164

Henley CL (1991) Cell geometry for cluster-based quasicrystal models. Phys Rev B 43:993

Hiraga K, Sun W (1993) The atomic arrangement of an Al–Pd–Mn decagonal quasicrystal studied by high-resolution electron microscopy. Philos Mag Lett 67:117

Hiraga K, Abe E, Matsuo Y (1994) The structure of an Al–Pd decagonal quasicrystal studied by high-resolution electron microscopy. Philos Mag Lett 70:163

https://icsd.fiz-karlsruhe.de

https://matdata.asminternational.org

Krajčí M, Windisch M, Hafner J, Kresse G, Mihalkovič M (1995) Atomic and electronic structure of icosahedral Al–Pd–Mn alloys and approximant phases. Phys Rev B 51:17355. https://doi.org/10.1103/PhysRevB.51.17355

Kreiner G, Franzen H (1997) The crystal structure of λ-Al_4Mn. J Alloys Compd 261:83

Kresse G, Furthmuller J (1996) Efficient iterative schemes for ab initio total-energy calculations using a plane-wave basis set. Phys Rev B 54:11169

Kresse G, Joubert D (1999) From ultrasoft pseudopotentials to the projector augmented-wave method. Phys Rev B 59:1758

Li M, Li C, Wang F, Zhang W (2006) Thermodynamic assessment of the Al–Pd system. Intermetallics 14:39

Matkovic T, Schubert K (1977) Kristallstruktur von PdAl. J Less Common Met 55:45

Mihalkovič M, Henley CL (2012) Empirical oscillating potentials for alloys from ab initio fits and the prediction of quasicrystal-related structures in the Al–Cu–Sc system. Phys Rev B 85:092102

Mihalkovič M, Henley CL (2013) Caged clusters in $Al_{11}Ir_4$: structural transition and insulating phase. Phys Rev B 88:064201. https://doi.org/10.1103/PhysRevB.88.064201

Mihalkovič M, Widom M (2004) Ab-initio cohesive energies of Fe-based glass-forming alloys. Phys Rev B 70:144107

Mihalkovič M, Widom M (2012) Structure and stability of Al_2Fe and Al_5Fe_2: first-principles total energy and phonon calculations. Phys. Rev. B 85:014113

Mihalkovič M, Widom M (2020) Spontaneous formation of thermodynamically stable Al-Cu-Fe icosahedral quasicrystal from realistic atomistic simulations. Phys Rev Res 2:013196

Mihalkovič M, Krajčí M, Widom M (2013) Prediction of stable insulating intermetallic compounds. Phys Rev B 87:100201

Mihalkovič M, Roth J, Trebin H-R (2017) Atomic structure of a decagonal Al–Pd–Mn phase. Phys Rev B 96:214103

Mihalkovic M, Widom M (2023) Al-Mn-Pd. http://alloy.phys.cmu.edu/published/. Accessed 30 May 2023

Okamoto H (1993) Mn–Pd (Manganese–Palladium). J Phase Equilib 14:654

Okamoto H (2003) Al–Pd (Aluminum–Palladium). J Phase Equilib 24:196

Okamoto H, Massalski T (1991) Thermodynamically improbable phase diagrams. J Phase Equilib 12:148

Perdew JP, Burke K, Ernzerhof M (1996) Generalized gradient approximation made simple. Phys Rev Lett 77:3865

Quandt A, Elser V (2000) Ab initio based modeling of i-AlPdMn. Phys Rev B 61:9336. https://doi.org/10.1103/PhysRevB.61.9336

Rodic D, Ahlzen P, Andersson Y, Tellgren R, Bouree VF (1991) The crystal and magnetic structure of tetragonal Pd3Mn. Solid State Commun 78:767

Shechtman D, Blech I, Gratias D, Cahn J (1984) Metallic phase with long-range orientational order and no translational symmetry. Phys Rev Lett 53:1951

Shi NC, Li XZ, Ma ZS, Kuo KH (1994) Crystalline phases related to a decagonal quasicrystal. I. A single-crystal X-ray diffraction study of the orthorhombic Al_3Mn phase. Acta Crystallogr Sect B 50:22

Shoemaker CB, Keszler DA, Shoemaker DP (1989) Structure of μ-$MnAl_4$ with composition close to that of quasicrystal phases. Acta Crystallogr Sect B 45:13

Simura R, Kaji N, Sugiyama K, Hiraga K (2011) Crystal structure of a new orthorhombic Al72Pd18Mn5Si5 approximant phase. Philos. Mag. 91:2603

Thimmaiah S, Tener Z, Lamichhane TN, Canfield PC, Miller GJ (2017) Crystal structure, homogeneity range and electronic structure of rhombohedral gamma-Mn5Al8. Z Krist 232:601

Wolverton C, Ozoliņš V (2001) Entropically favored ordering: the metallurgy of Al_2Cu revisited. Phys Rev Lett 86:5518

Zijlstra ES, Bose SK, Klanjšek M, Jeglič P, Dolinšek J (2005) Ab initio study of icosahedral Al–Pd–Mn quasicrystals: structural model, electric field gradients, and negative valence of Mn. Phys Rev B 72:174206. https://doi.org/10.1103/PhysRevB.61.9336